

# LEGIBILITY NOTICE

A major purpose of the Technical Information Center is to provide the broadest dissemination possible of information contained in DOE's Research and Development Reports to business, industry, the academic community, and federal, state and local governments.

Although a small portion of this report is not reproducible, it is being made available to expedite the availability of information on the research discussed herein.

CONF-8706166--4

1987 06 16

Los Alamos National Laboratory is operated by the University of California for the United States Department of Energy under contract W-7405-ENG-36

TITLE: PION SINGLE- AND DOUBLE-CHARGE-EXCHANGE REACTIONS AT LOW ENERGIES

LA-UR--87-3367

DE88 001841

AUTHOR(S): Helmut W. Baer, MP-4

SUBMITTED TO: Proceedings of the International Symposium on Medium Energy Physics, June 23-27, 1987, Beijing, China

DISCLAIMER

This report was prepared as an account of work sponsored by an agency of the United States Government. Neither the United States Government nor any agency thereof, nor any of their employees, makes any warranty, express or implied, or assumes any legal liability or responsibility for the accuracy, completeness, or usefulness of any information, apparatus, product, or process disclosed, or represents that its use would not infringe privately owned rights. Reference herein to any specific commercial product, process, or service by trade name, trademark, manufacturer, or otherwise does not necessarily constitute or imply its endorsement, recommendation, or favoring by the United States Government or any agency thereof. The views and opinions of authors expressed herein do not necessarily state or reflect those of the United States Government or any agency thereof.

By acceptance of this article, the publisher recognizes that the U.S. Government retains a nonexclusive, royalty-free license to publish or reproduce the published form of this contribution, or to allow others to do so, for U.S. Government purposes.

The Los Alamos National Laboratory requests that the publisher identify this article as work performed under the auspices of the U.S. Department of Energy

Los Alamos Los Alamos National Laboratory Los Alamos, New Mexico 87545

# PION SINGLE- AND DOUBLE-CHARGE-EXCHANGE REACTIONS AT LOW ENERGIES†

*Helmut W. Baer*  
*Los Alamos National Laboratory*

## ABSTRACT

The general features of pion charge-exchange reactions at energies of 20 to 80 MeV leading to nuclear isobaric-analog states (IAS) and double-isobaric-analog states (DIAS) are reviewed. The recent progress achieved in understanding the role of short-range N-N correlations in the double-charge-exchange reactions is presented.

## I. INTRODUCTION

Low-energy pion-nucleus interactions are distinct from the higher-energy ( $T_\pi > 80$  MeV) reactions in that there is considerable penetration into the nuclear interior due to the relatively weak pion-nucleon coupling and the relatively small pion-absorption cross sections. Second, only the s- and p-partial waves are significant in the  $\pi - N$  interaction. In the charge-exchange reaction, these two partial-wave amplitudes interfere destructively at forward scattering angles, causing a near-vanishing of the cross section at 50 MeV. These features of the single-charge-exchange reaction have some interesting consequences for forward-angle double charge exchange. Specifically, they appear to enhance the role of short-range N-N components in nuclear wave functions in forward-angle DCX reactions. We discuss the recent work supporting this conclusion in this article.

Of all the states produced in pion charge-exchange reactions, two play a special role: the isobaric-analog state (IAS) and the double-isobaric-analog state (DIAS). These states are in the same isospin multiplet as the target ground state and are reached in pion single- and double-charge-exchange reactions. In transitions to these states nuclear structure uncertainties are reduced to an absolute minimum. Also, in the charge-exchange reactions, Coulomb effects play only a minor role, even at low energies, which renders the cross sections directly sensitive to the hadronic interactions. This is unlike elastic scattering,

---

† Invited talk given at the International Symposium on Medium Energy Physics, June 23-27, Beijing, The People's Republic of China

where Coulomb effects are often quite large. The IAS transitions allow for study of medium modifications on the elementary  $\pi^+n \rightarrow \pi^0p$  process and the distorted-wave effects in the  $\pi - A$  interaction. This leaves the double-scattering mechanism as the primary phenomenon to be studied in the DIAS transitions. It is these transitions that are unique to pion scattering and that we wish to utilize for investigating nucleon correlations in nuclei.

## II. PION SINGLE CHARGE EXCHANGE, 20 TO 80 MeV

### A. The Elementary $\pi - N$ Charge-Exchange Reaction

We examine first the behavior of the elementary  $\pi^-p \rightarrow \pi^0n$  reaction (Ref. 1). The angular distributions for energies 50, 180, and 425 MeV are shown in Fig. 1. At 180 MeV

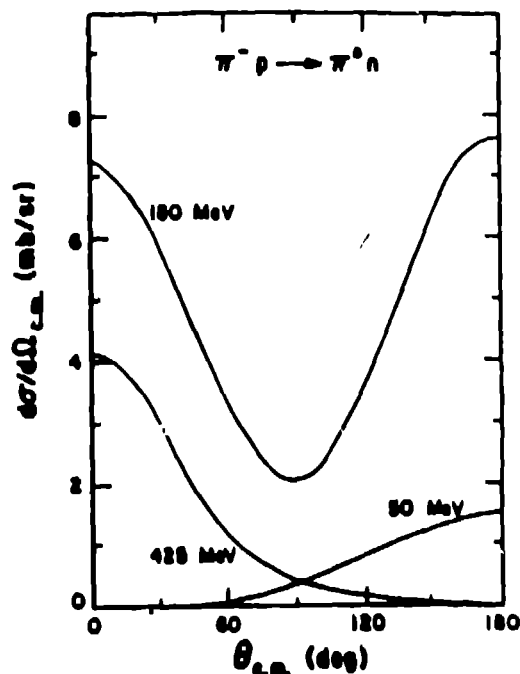


Fig. 1. Angular distributions for the  $\pi^-p \rightarrow \pi^0n$  reactions at three energies, as given by a current phase-shift analysis (Ref. 1).

the angular distribution is nearly symmetric at  $90^\circ$ , a consequence of having nearly pure  $p$ -wave scattering, which gives an angular dependence of  $(1 + \cos^2\theta)$ . This feature was useful in identifying the quantum numbers of the  $\Delta$  in the early 1950's. At 425 MeV, and at higher energies, the angular distributions are sharply forward-peaked. At this energy  $d$  and  $f$  partial waves are beginning to become significant. At 50 MeV the angular distribution is backward peaked, and it has a nearly vanishing cross section at  $0^\circ$ , a consequence of the interference in  $s$  and  $p$  partial waves.

The energy dependence of this s-p wave interference phenomenon is shown in Figs. 2 and 3. In Fig. 2, the angular distributions at energies 10, 50, and 80 MeV are shown.

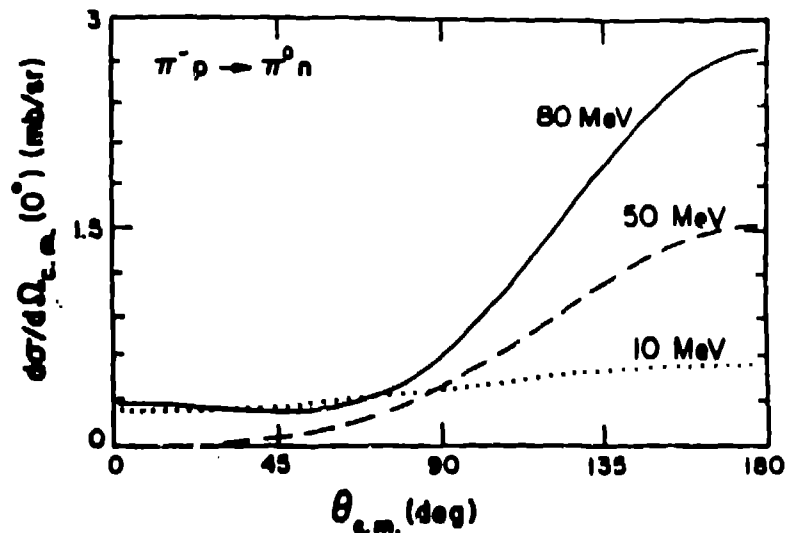


Fig. 2. Angular distributions for the  $\pi^- p \rightarrow \pi^0 n$  reactions at three low energies (Ref. 1).

We see that over the energy interval (10 to 80 MeV) pion single-charge exchange is depressed at forward angles. This is also shown in Fig. 3, which shows the  $0^\circ$  cross section as a function of pion energy. For energies up to 100 MeV, forward-angle single charge exchange is quite small, with cross sections  $\lesssim 0.5$  mb/sr.

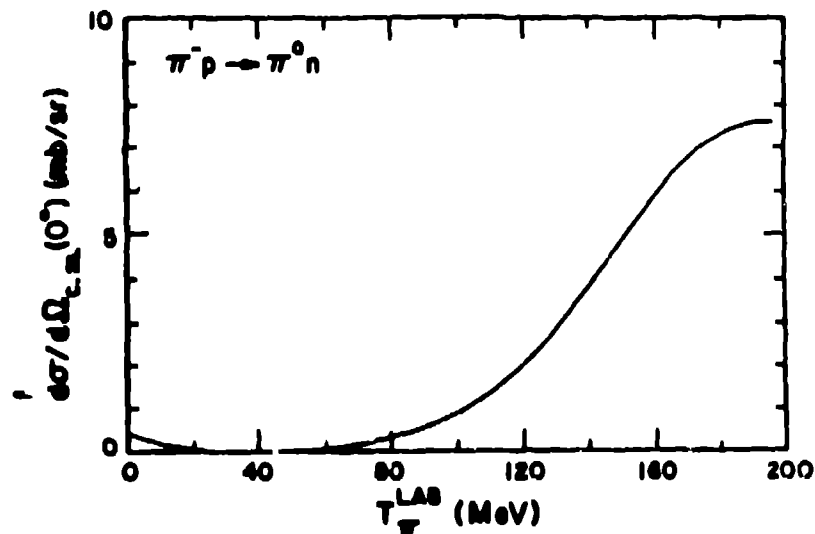


Fig. 3. The  $0^\circ$  cross sections as a function of incident energy for the  $\pi^- p \rightarrow \pi^0 n$  reaction (Ref. 1).

The  $\pi^-p \rightarrow \pi^0n$  cross sections at low energies were recently measured<sup>2</sup> with the  $\pi^0$  spectrometer in Los Alamos and at TRIUMF with NaI detectors. A report of this work and the consequences for phase-shift analyses may be found in the talk given at this Symposium by Professor Measday<sup>3</sup>.

### B. Nuclear IAS Transitions

Using the  $\pi^0$  spectrometer<sup>4</sup> at LAMPF we have made extensive measurements of IAS cross sections at energies in the 20 to 80 MeV interval. What we have learned from these data is that many features of the elementary  $\pi N$  charge-exchange cross sections are quite closely reflected in the nuclear IAS cross sections. The sharpest feature is the near-vanishing of the  $0^\circ$  cross section around 50 MeV. This is nicely observed in the set of spectra shown in Fig. 4 for the  $^{14}\text{C}(\pi^+, \pi^0)$  reaction at energies 35 to 100 MeV<sup>5</sup>. The

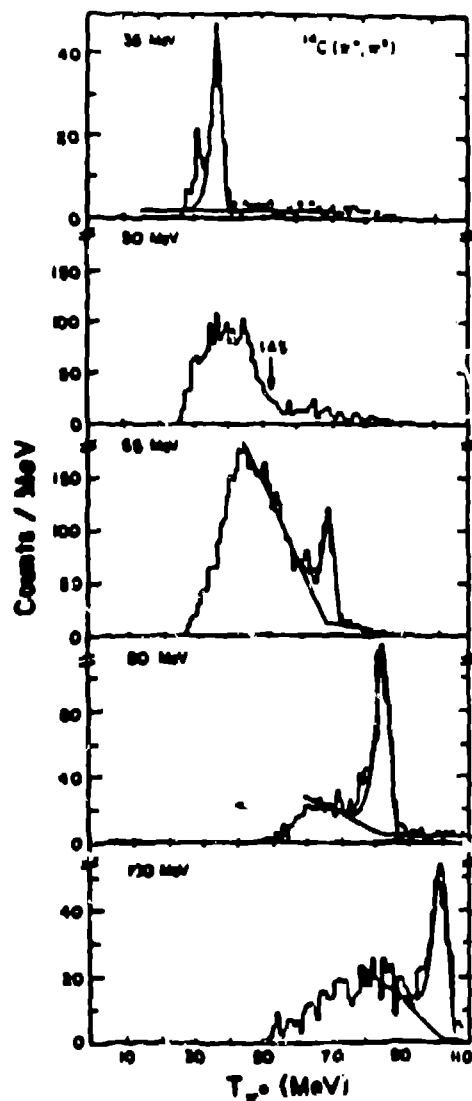


Fig. 4. Spectra for the  $^{14}\text{C}(\pi^+, \pi^0)$  reaction measured<sup>5</sup> at forward angles (0 to  $10^\circ$ ) at different energies. The IAS is seen to disappear at 50 MeV.

IAS disappears at 50 MeV, whereas it stands out prominently at the other energies. The measured  $0^\circ$  cross sections are shown in Fig. 5, where they are compared to

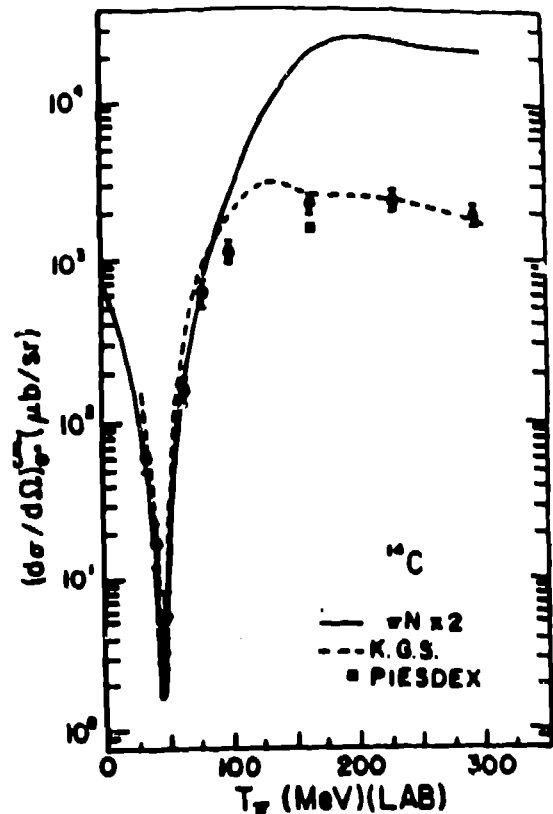


Fig. 5. The energy dependence of  $0^\circ$  IAS cross sections on  $^{14}\text{C}$  (Ref. 5). The solid line represents two times the free  $\pi^-p \rightarrow \pi^0n$  cross section. The dashed line represents the multiple scattering theory calculations of Kaufmann et al. as discussed in Ref. 5.

$2 \times d\sigma/d\Omega(\pi^-p \rightarrow \pi^0n)$ . They closely track this curve for energies up to 80 MeV. At higher energies, pion absorption plays a much larger role, and the nuclear cross sections fall well below the free cross section.

The sharp dip in the  $0^\circ$  excitation function was seen<sup>6</sup> in the nuclei from  $^7\text{Li}$  to  $^{120}\text{Sn}$ . The data are shown in Fig. 6. The curves represent polynomial functions fit to the data to locate the positions of the minima. The persistence of the sharp-dip structure in the IAS transition shows that the dispersive-medium effects are small at low pion energies. In a distorted-wave Born-approximation description, the IAS scattering amplitude is expressed as a transition between incoming and outgoing distorted waves. Since the distortions

arise primarily from the isoscalar part of the optical potential, which is not strongly energy dependent at low pion energies, the measured  $0^\circ$  cross sections should reflect the energy dependence of the medium-modified charge-exchange transition operator. Thus the observed similarity between the free-charge-exchange and the nuclear-IAS-transition cross sections indicates that the energy dependence of the isovector pion-nucleon interaction is not strongly modified by the nuclear medium. This important result obtained in the low-energy IAS measurements allows one to proceed with greater confidence in the analyses of low-energy DCX scattering.

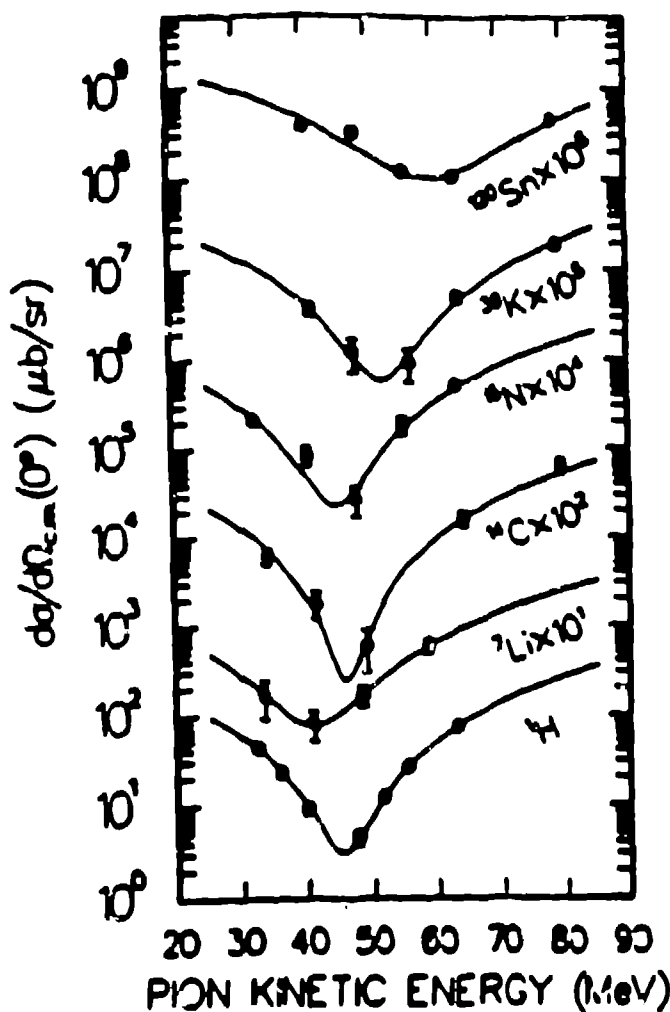


Fig. 8. The measured  $0^\circ$  excitation functions for the IAS transition at low pion energies.<sup>6</sup> The solid lines represent polynomial fits to the data used to determine the energy of the minima in the cross sections.

Further similarity of nuclear IAS transition with the  $\pi^-p \rightarrow \pi^0n$  reaction is seen in the angular distribution shapes.<sup>5-8</sup> At forward angles these have quite similar shapes. Some representative data on the  $^{15}\text{N}$  IAS transition at 55.5, 48.2, and 33.4 MeV are shown in Fig. 7. Data at 20 MeV are shown in Fig. 8 for  $^7\text{Li}$  and  $^{14}\text{C}$ . The general shapes of

these angular distributions follow plane-wave model calculations as shown explicitly in Ref. 5 for  $^{14}\text{C}$ , and as can be seen from the  $\pi^-p \rightarrow \pi^0n$  cross sections shown in Fig. 2.

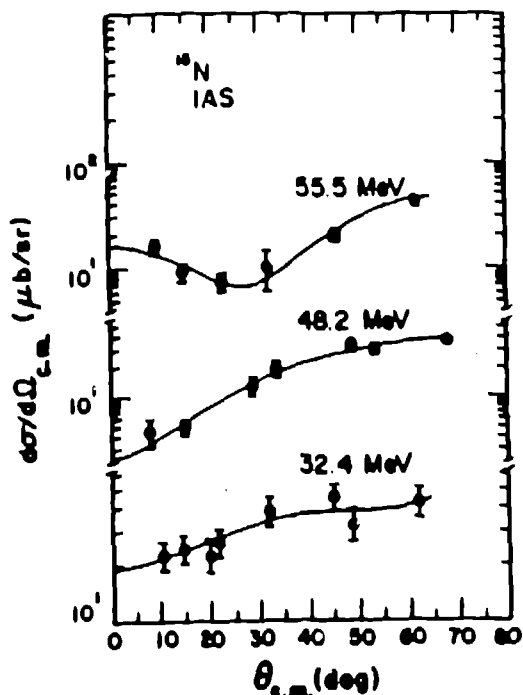


Fig. 7. Angular distributions for the IAS transition on  $^{15}\text{N}$  at three low energies.<sup>6,7</sup> The curves represent the polynomial function fits to the data used to determine  $0^\circ$  cross sections.

Data at 20 MeV now exist<sup>8</sup> for  $^7\text{Li}$ ,  $^{14}\text{C}$ ,  $^{15}\text{N}$ ,  $^{60}\text{Ni}$ , and  $^{120}\text{Sn}$  at forward scattering angles. For  $^7\text{Li}$  we were able to measure cross sections near  $180^\circ$  as shown in Fig. 8. These demonstrate the near isotropy of the angular distributions. A second point investigated in this study<sup>8</sup> was the role of Coulomb distortions in the incoming  $\pi^+$  wave in modifying

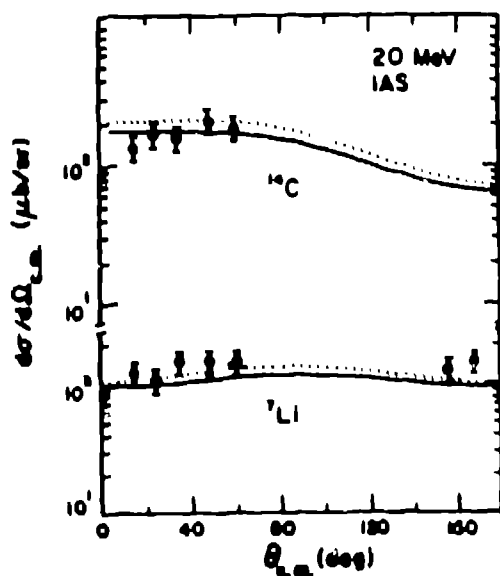


Fig. 8. Angular distributions at 20 MeV for the IAS transitions on  $^7\text{Li}$  and  $^{14}\text{C}$  (Ref. 8). The solid curves are DWIA calculations including the Coulomb force on the incident pion. The dotted curve is for the same calculations with the Coulomb force turned off.

IAS cross sections. We see in Fig. 8 that even at 20 MeV, this effect is quite small. This contrasts with inelastic  $\pi^+$  and  $\pi^-$  scattering at low pion energies where Coulomb distortions play a major role.

The conclusions we draw from the low-energy IAS data are: (1) the net medium effects are small in IAS transitions; (2) DWIA calculations give a good overall representation of the data; (3) the role of Coulomb distortion is small.

### III. PION DOUBLE CHARGE EXCHANGE, 20 TO 80 MeV

#### A. The $^{14}\text{C}$ Puzzle

We have seen that for  $^{14}\text{C}$  and for other nuclei the IAS cross sections have a minimum near 50 MeV. In view of the behaviour of IAS cross sections at 50 MeV, it came as a considerable surprise when Miller<sup>9</sup> predicted a large  $0^\circ$  cross section of  $12 \mu\text{b}/\text{sr}$  for the  $^{14}\text{C}$  DIAS transition at 50 MeV. At higher energies the DIAS cross sections are typically  $\lesssim 1 \mu\text{b}/\text{sr}$ .

Miller's prediction was based on a hybrid quark-nucleon model designed to deal with short-range  $N - N$  components found in ordinary nuclear wave functions. In this model, two nucleons lose their separate identities when they come close together, forming a six-quark cluster. The probability for this is governed by  $r_0$ , the two-nucleon separation distance. Miller used the value  $r_0 = 0.95$  fm, which gives a six-quark cluster probability of 6% for  $^{14}\text{C}$ . To calculate the scattering amplitude the pions are coupled directly to the quarks inside the bag via an axial-vector operator of the form

$$g_{\pi N} \vec{\sigma}_j \cdot \vec{k}_\pi \tau_+$$

where  $\vec{\sigma}_j$  is the quark spin operator,  $\vec{k}_\pi$  is the pion momentum,  $\tau_+$  is the charge-changing operator, changing a down quark to an up quark, and  $g_{\pi N}$  is the experimentally determined pion-nucleon coupling constant.

The results of Miller's predictions<sup>9</sup> are compared with the LAMPF data<sup>10</sup> in Fig. 9. The pronounced forward peak is certainly seen in the data, although the measured  $0^\circ$  cross section of  $3.9 \pm 0.4 \mu\text{b}/\text{sr}$  is less than predicted. Miller subsequently<sup>11</sup> corrected his original plane-wave calculation by including a pion absorption factor of  $\exp(\ell/\lambda)$ , which lowered the  $0^\circ$  cross section to  $4 \mu\text{b}/\text{sr}$ .

Optical-potential calculations based on sequential scattering through the analog intermediate state considerably underestimate the forward-angle cross section. A representative calculation is shown in Fig. 9.

This situation prompted Gibbs, Kaufmann, and Siegel<sup>12</sup> to calculate both IAS and DIAS cross sections for  $^{14}\text{C}$  using their multiple scattering theory. With their model they could give detailed information on the range and angles involved for the intermediate pion propagation. They gave a geometrical answer as to how SCX could be small at  $0^\circ$  and DCX could be large. It was two  $90^\circ$  SCX scatterings that gave a large  $0^\circ$  DIAS cross section. The distance traveled by the intermediate  $\pi^0$  was also calculated, and they obtained the result that approximately 50% of the scattering amplitude arose from scatterings where the two nucleons were within 1 fm of each other. Thus, their calculations lent support to Miller's contention that large DIAS cross sections at  $0^\circ$  signified a large role of short-range  $N$ - $N$  components.

Higher-order optical-potential treatments by Siciliano *et al.*<sup>13,14</sup> and Liu<sup>15</sup> were also able to reproduce the IAS and DIAS cross sections. The higher-order terms are thought to represent short-range effects.

A different conclusion was reached by Karapiperis and Kobayashi,<sup>16</sup> who used the  $\Delta$ -hole model to calculate the IAS and DIAS cross sections for  $^{14}\text{C}$ . They claimed that the DIAS transition does not involve appreciable contributions from short-range  $N$ - $N$  correlations.

Considerable effort has gone into resolving this question. We will review these results. They suggest a tentative answer.

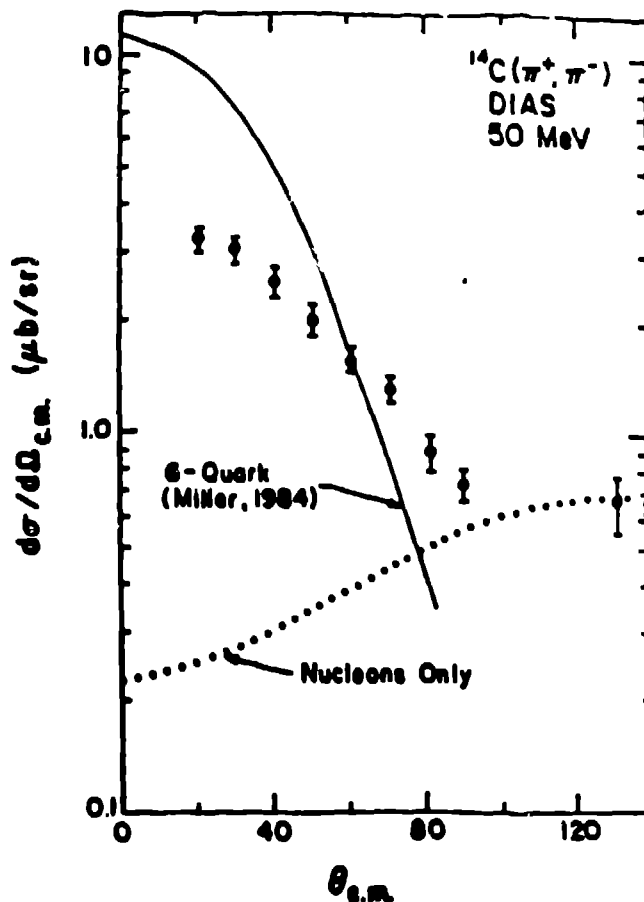


Fig. 9. Differential cross sections for the DIAS transition on  $^{14}\text{C}$ . The data and the dotted curve are from Ref. 10. The solid curve is from Ref. 9.

## B. DCX Mechanisms

The classification of DCX mechanisms is less than straightforward because different theoretical formulations are used to describe the same phenomena. There are at least six distinct approaches:

1. Optical-potential phenomenology (e.g., Refs. 14, 15, 17, and 18).
2. Multiple-scattering treatments (e.g., Ref. 12).
3. Glauber model (e.g., Ref. 19).
4.  $\Delta$ -hole model (e.g., Refs. 16 and 20).
5. Meson-exchange currents (e.g., Ref. 21).
6. Six-quark bags (e.g., Refs. 9 and 22).

Since we are interested in determining what the range of double scattering is, and particularly we would like to see if the short-range  $N$ - $N$  dynamics of DCX reactions can be isolated, the problem is to determine whether the various approaches reach the same answer on this point.

A basic distinction in the approaches is whether they assume *sequential scattering* or some *specialized short-range DCX mechanism*. By sequential scattering, we mean that the  $\pi^+$  of the beam charge exchanges on a neutron to produce a  $\pi^0$ , which propagates to another neutron where it charge exchanges to produce a  $\pi^-$ , which then leaves the nucleus and is detected. This process can be broken into two contributions, depending on whether the intermediate nuclear state is the IAS or whether it is a set of other states. This picture for sequential scattering is illustrated in Fig. 10.

Some explicitly short-range DCX mechanisms are illustrated in Fig. 11. These give a quite different picture of DCX. In the six-quark bag picture, two neutrons momentarily form a six-quark bag. While in this condition, a  $\pi^+$  is absorbed and a  $\pi^-$  is emitted, converting two down quarks to two up quarks. In the  $\Delta$ -interaction (DINT) diagram a neutron accepts the  $\pi^+$  and later, after brushing off a  $\pi^+$ , radiates a  $\pi^-$ . This resembles elastic scattering on a single nucleon. In the meson-exchange process, the  $\pi^+$  beam double-charge exchanges on a virtual pion in transit between two nucleons. All three of these processes are manifestly short-range processes.

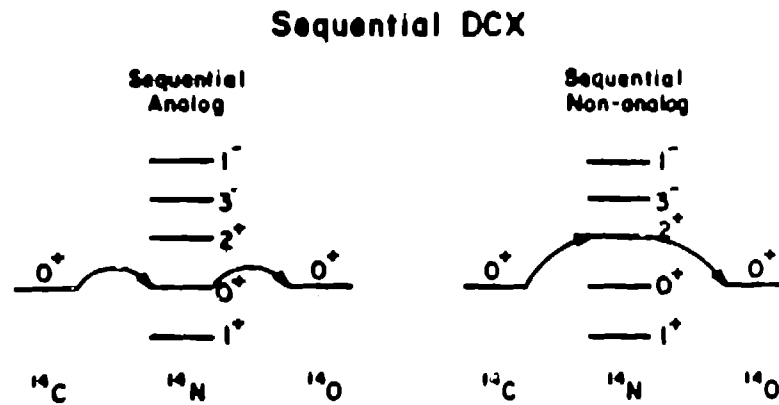


Fig. 10. Illustration of the two types of sequential scattering involved in DIAS transitions.

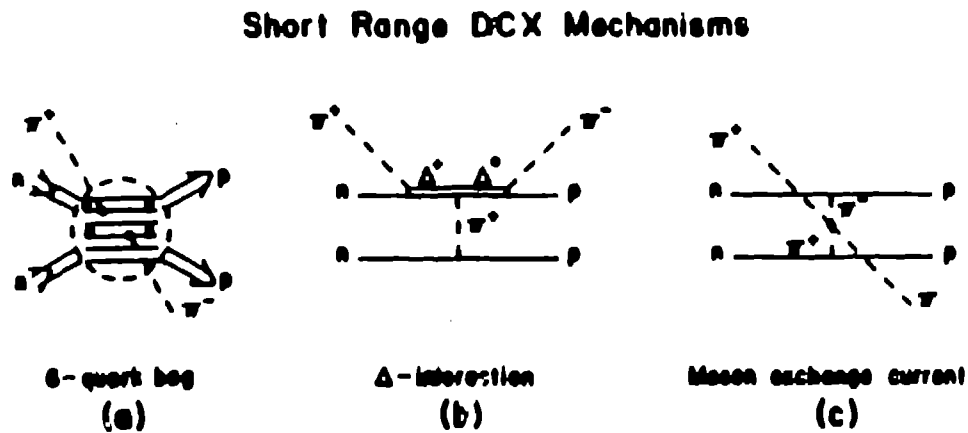


Fig. 11. Illustration of short-range DCX mechanisms discussed in the text.

The sequential scattering processes discussed above may also contain short-range components. In fact, we have already noted that the sequential scattering calculations of Gibbs *et al.*<sup>12</sup> explicitly show short-range components. Fruitful investigations of sequential scattering have occurred in the past year, and we now turn to a discussion of these results.

### C. Sequential Scattering Treatments

Bleszynski and Glauber<sup>23</sup> have just completed a detailed analysis of the IAS and DIAS transitions in  $^{14}\text{C}$  using a sequential scattering picture. Their study is particularly instructive regarding the role played by the spatial correlations in the valence nucleons. As a general result, they find that the correlations contained within proven shell-model wave functions are adequate to give a satisfactory account of both the IAS and DIAS transitions at 50 MeV. Their calculations are compared with the data in Fig. 12. For these calculations the Cohen and Kurath wave functions<sup>24</sup> for the  $^{14}\text{C}$  ground state were employed. The role of distortions was found to be minimal. The two sets of curves represent plane-wave impulse approximation calculations and distorted-wave impulse-approximation calculations.

The Cohen-Kurath wave functions evidently contain the correct spatial correlations. In an LS coupling scheme, as used in Ref. 23, there are only two components in the  $^{14}\text{C}$  wave function,

$$|^{14}\text{C}, \text{g.s.}\rangle = \alpha |^1S_0\rangle + \beta |^3P_0\rangle,$$

assuming that only  $p$ -shell nucleons are active. The calculations shown in Fig. 12 used values  $|\alpha| = 0.85$  and  $|\beta| = 0.52$  corresponding to the Cohen-Kurath values. The IAS angular distribution would have looked quite different for  $\alpha = 1$  or for  $\beta = 1$  as is shown in Fig. 13. The forward peaking of the angular distribution is due to the  $^1S_0$  component. In this state of relative motion the nucleons can move on top of each other ( $\vec{r}_1 \approx \vec{r}_2$ ), whereas in the  $^3P_0$  state, which is spatially antisymmetric, the wave function vanishes

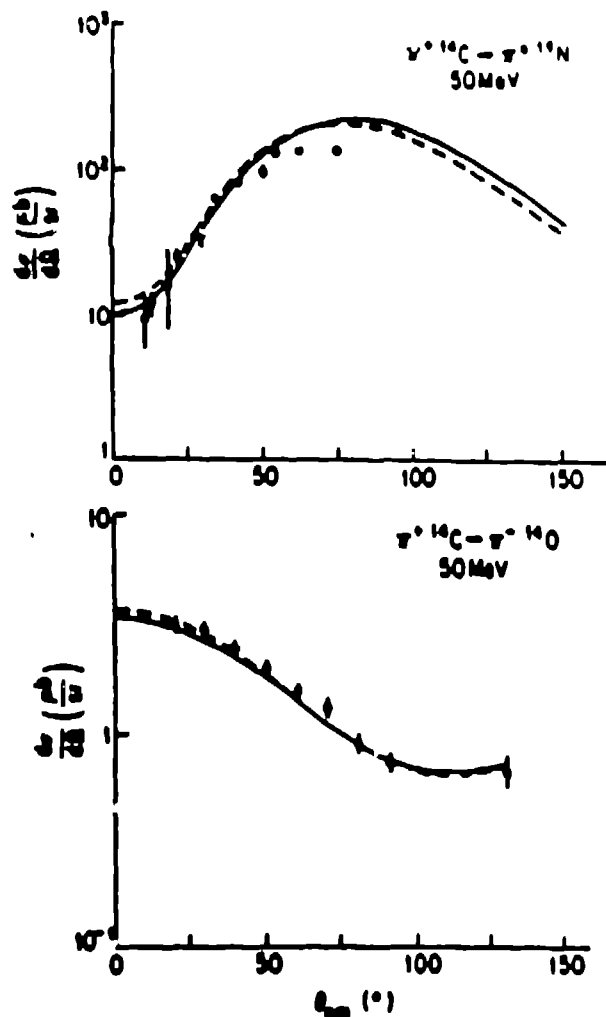


Fig. 12. Comparison of the calculations of Bleszynski and Glauber<sup>23</sup> with the  $^{14}\text{C}$  data on the IAS and DIAS transitions (Refs. 5 and 10). The dashed and solid curves correspond to plane-wave and distorted-wave calculations, respectively.

for  $\vec{r}_1 = \vec{r}_2$ . Thus, pronounced forward peaking is seen to be a signature of short-range spatial correlations.

Bleszynski and Glauber investigated this point more quantitatively by expressing the double-scattering amplitude in terms of the relative coordinate  $\vec{r} = \vec{r}_1 - \vec{r}_2$  and centroid coordinate  $\vec{R} = \frac{1}{2}(\vec{r}_1 + \vec{r}_2)$ . The factor which contains the dependence on the relative coordinate is  $\Omega(\vec{r}, \vec{R}, \Lambda)$ . The averaged and weighted value of this function, so as to reflect appropriately the dependence on internucleon distance  $r$ , is displayed in Fig. 14. This curve shows that most of the DCX occurs at distances smaller than 2 fm and that the most probable distance of separation is 1.2 fm. These results are quite consistent with the earlier results of Gibbs *et al.*<sup>12</sup> In view of the fact that the rms charge radius of the proton is 0.84 fm, one would have to conclude that there is considerable overlap of the two nucleons as they are converted from neutrons to protons.

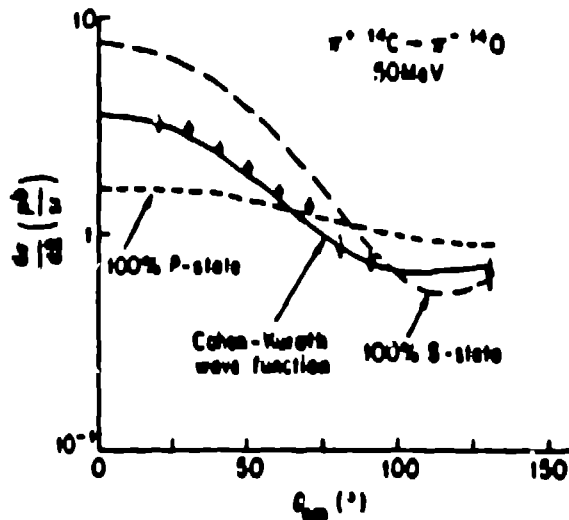


Fig. 13. Comparison of the  $^{14}\text{C}$  data with calculations<sup>23</sup> using different model wave functions, as discussed in the text.

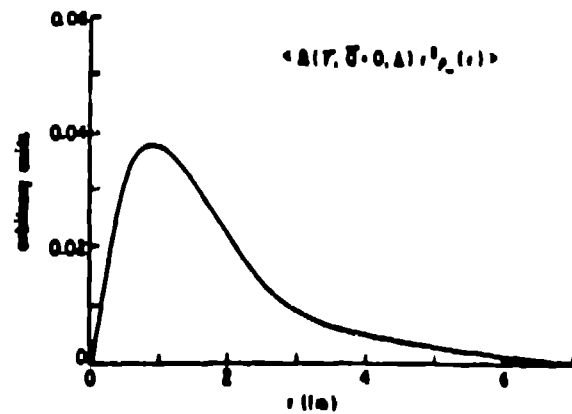


Fig. 14. The function  $|\Omega(\vec{r}, \vec{Q} = 0; \Lambda)| r^2 \rho(r)$  as defined in Ref. 23, with  $\Lambda = 3.5 \text{ fm}^{-1}$ , and averaged over orientations of  $\vec{r}$  (see text).

A further result given by Bleszynski and Glauber is an evaluation of the role of the IAS intermediate state. For the full DIAS amplitude, they summed over all accessible intermediate states (closure). When only the IAS intermediate state is included, they obtain a flat angular distribution, as is shown in Fig. 15. They point out that restricting the intermediate state to the IAS corresponds to omitting  $N-N$  correlations.

The large role of nonanalog intermediate states at 50 MeV for the  $^{14}\text{C}$  DIAS transitions was noted earlier in Refs. 12 and 16. Calculations with optical potentials<sup>14,15</sup> also point to a large role of nonanalog intermediate states.

Thus, three points emerge from analyses of the  $^{14}\text{C}$  data: (1) forward-angle DIAS cross sections at 50 MeV arise predominantly from scatterings through nonanalog intermediate states; (2)  $N$ - $N$  correlations are responsible for the transitions through the nonanalog intermediate states; and (3) most DIAS transition strength involves nucleon correlations with  $r < 2$  fm.

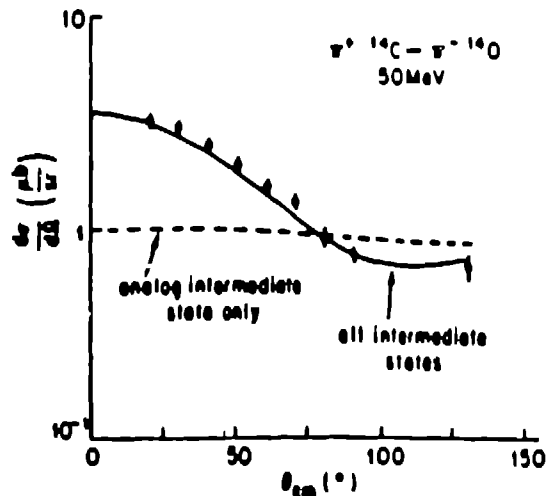


Fig. 15. Comparison of the  $^{14}\text{C}$  DIAS data with calculations of Ref. 23. The dashed curve results when only the IAS intermediate state is included; the solid curve results from a sum over all intermediate states.

#### D. DIAS Transitions on $^{42,44,48}\text{Ca}$

The Ca isotopes offer an attractive opportunity to study further the effects of nucleon correlations. To this end we measured<sup>25,26</sup> the isotopes Ca-42,44,48, which have 2, 4, and 8 valence neutrons in the  $1f_{7/2}$  shell, respectively. Our initial, naive expectation, before we fully appreciated the large role played by  $N$ - $N$  correlations, was that the cross sections would increase with the addition of valence neutrons. This was based on the apparent success of the low-energy plane-wave model of Koltun and Reitan,<sup>27</sup> which predicts a  $(N - Z)(N - Z - 1)$  dependence and a very weak  $A$ -dependence. This model explained the near-constancy of the measured 50-MeV cross sections for the  $T = 1$  nuclei  $^{14}\text{C}$ ,  $^{16}\text{O}$ , and  $^{26}\text{Mg}$ . In our first run on  $^{48}\text{Ca}$  we were quite surprised to learn that the  $^{48}\text{Ca}$  cross section has about the same value as that of  $^{14}\text{C}$ . Since the factor  $(N - Z)(N - Z - 1)$  is 28 times larger for  $^{48}\text{Ca}$  than for  $^{14}\text{C}$ , this result was quite puzzling. It looked like a significant  $A$ -dependence had developed at  $A > 26$ . In our second run we measured  $^{42,44}\text{Ca}$  and found  $^{44}\text{Ca}$  to have about one-half the cross section of  $^{42}\text{Ca}$ . The spectra are shown in Fig. 10 and the cross sections are given in Table I. This result showed convincingly that  $A$ -dependence was not the dominant effect. It was highly suggestive of an interference effect having its origin in shell-model correlations.

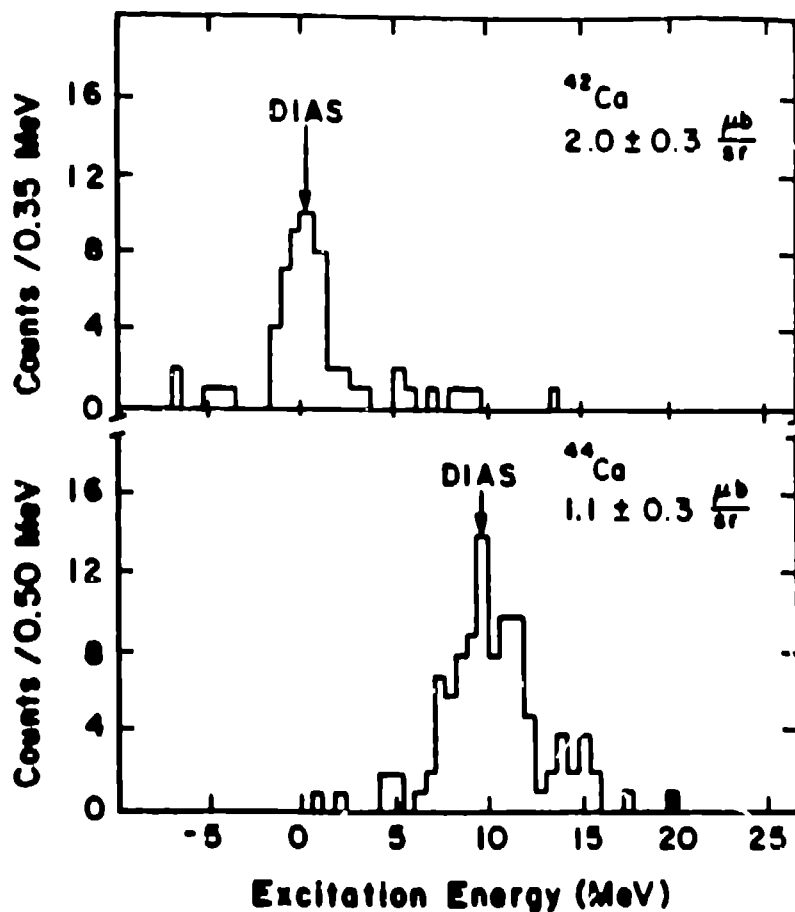


Fig. 16. Measured spectra<sup>25,26</sup> for the  $^{42,44}\text{Ca}(\pi^+, \pi^-)$  reactions at 35 MeV and  $40^\circ$ .

Table I. The measured laboratory cross sections for the calcium isotopes at a laboratory scattering angle of  $40^\circ$  (Refs. 25 and 20).

Isotope	$T_\pi^a$ (MeV)	$d\sigma/d\Omega$ ( $\mu\text{b}/\text{sr}$ )	Relative Uncertainties <sup>b</sup> ( $\mu\text{b}/\text{sr}$ )
$^{42}\text{Ca}$	33.6	$2.0 \pm 0.5$	( $\pm 0.3$ )
$^{44}\text{Ca}$	32.0	$1.1 \pm 0.3$	( $\pm 0.15$ )
$^{46}\text{Ca}$	34.2	$2.4 \pm 0.7$	( $\pm 0.0$ )

<sup>a</sup>Kinetic energy at the center of the target.

<sup>b</sup>Relative uncertainties appropriate for the isotopic comparison.

By this time E. Bleszynski, M. Bleszynski, and Glauber had begun calculations which showed that there were large differences in the two-body correlation densities in  $(f_{7/2})^n$  configurations for different values of  $n$ . A comparison of  $^{42}\text{Ca}$  and  $^{48}\text{Ca}$  is shown in Fig. 17 (Ref. 28). What is plotted is the "separation density" which is defined by

$$\rho_{\text{sep}}(\vec{r}) = \int d^3R \rho^{(2)}(\vec{R} + \vec{r}/2, \vec{R} - \vec{r}/2)$$

with

$$\rho^{(2)}(\vec{r}_1, \vec{r}_2) = \rho^{(1)}(\vec{r}_1)\rho^{(1)}(\vec{r}_2)[1 + C(\vec{r}_1, \vec{r}_2)] .$$

In these expressions  $\rho^{(2)}(\vec{r}_1, \vec{r}_2)$  is the two-particle density,  $\rho^{(1)}(\vec{r})$  is the single-particle density, and  $C(\vec{r}_1, \vec{r}_2)$  is the shell-model correlation function. To omit  $N$ - $N$  correlations corresponds to setting  $C = 0$ .

For the two valence nucleons of  $^{42}\text{Ca}$  (as well as  $^{14}\text{C}$ ), there is a large amount of spatial overlap in the two-particle wave function, giving an increased value of  $\rho_{\text{sep}}$  for small  $r$  (Fig. 17). For  $^{48}\text{Ca}$ , which has eight valence neutrons in a closed  $f_{7/2}$  shell, the Pauli exclusion principle enormously reduces  $\rho_{\text{sep}}$  at small  $r$ . For  $^{44}\text{Ca}$ ,  $\rho_{\text{sep}}(r)$  is intermediate to  $^{42}\text{Ca}$  and  $^{48}\text{Ca}$ . If indeed the DIAS transitions are most sensitive to the small  $r$  behavior of  $\rho_{\text{sep}}(r)$ , one can see a qualitative explanation for the behavior of the  $^{42,44,48}\text{Ca}$  cross sections. We discuss this below. Full calculations of the Ca cross sections taking into account the shell-model correlations and the  $\pi$ - $N$  interaction are now in progress.<sup>28,29</sup>

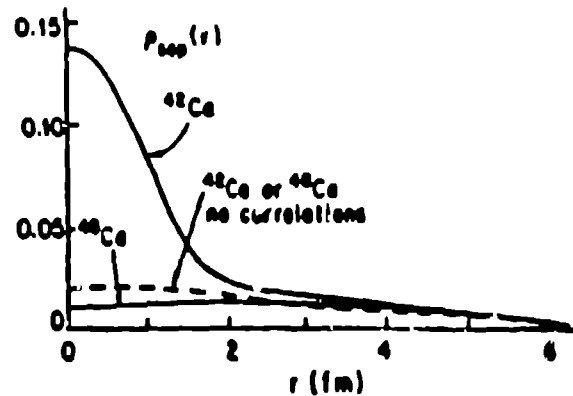


Fig. 17. Separation densities for  $(f_{7/2})^n$  configurations as given in Ref. 28.

### E. Two-Amplitude Shell Model

A useful formulation of the DIAS scattering amplitude in terms of analog and nonanalog components was given recently by Auerbach, Gibbs, and Plaszky.<sup>30</sup> If there are  $n$  neutrons in shell  $j$  and they are all coupled pairwise to  $J = 0$  (seniority = 0 configuration), the  $(\pi^+, \pi^-)$  DIAS cross section can be written as

$$\frac{d\sigma}{d\Omega_{\text{DIAS}}}(\theta) = \frac{(N-Z)(N-Z-1)}{2} |A(\theta) + \omega B(\theta)|^2$$

where the amplitude  $A$  represents the  $L = 0$  multipolarity of the two-body transition operator and the amplitude  $B$  represents a sum over all  $L \neq 0$  even multipoles. The weighting factor  $\omega$  for the  $B$  amplitude depends on  $N$  and  $Z$  according to

$$\omega = \frac{(2j + 3 - 2n)}{(n - 1)(2j - 1)},$$

where  $n = N - Z$ . We note that  $\omega$  has values 1, 1/9, -1/7 for Ca-42,44,48, respectively. We see that if  $|B| \gtrsim |A|$  there can be dramatic deviations from  $(N - Z)(N - Z - 1)$  scaling across the Ca isotopes.

Since the  $A$  amplitude represents the  $L = 0$  transition multipole, it represents predominantly the IAS intermediate state. (There may be small  $L = 0$  components in nonanalog states.) The  $B$ -term represents the sum over all nonanalog intermediate states. As we saw from the  $^{14}\text{C}$  analyses, there is considerable evidence that the forward-angle DIAS cross sections at 50 MeV derive most of their strength from nonanalog intermediate states. Thus we might expect  $|B| > |A|$ .

The data on the three Ca isotopes allow us to determine empirically  $|A|$ ,  $|B|$ , and the relative phase between  $A$  and  $B$ . The values determined from the data are given in Table II. The value  $|B| / |A| = 3.5$  is obtained. This implies that for  $^{42}\text{Ca}$ , where  $\omega = 1$ , the DIAS amplitude at  $40^\circ$  arises primarily from nonanalog intermediate states. For  $^{44}\text{Ca}$  and  $^{48}\text{Ca}$  the DIAS amplitudes arise predominantly from the IAS intermediate state, since the weighting factors of 1/9 and -1/7 greatly suppress the nonanalog amplitude. In terms of the  $N$ - $N$  correlations, we have seen from the calculations of Ref. 28 that  $\rho_{\text{sep}}(r)$  for  $^{42}\text{Ca}$  is large at small  $r$  and relatively flat for  $^{44,48}\text{Ca}$ . Thus, the Ca cross sections at low energy are quite naturally explained as a consequence of the  $N$ - $N$  correlations in  $(1f_{7/2})^n$  wave functions and the short-range nature of the double-scattering process.

Table II. The deduced magnitudes of  $A$ ,  $B$ , and  $\phi$  (relative phase angle) from the data in Table I. The units for  $A$  and  $B$  are  $(\mu\text{b})^{1/2}$ .

$ A $	$ B $	$\phi$	$ B  /  A $
0.34	1.45	$59^\circ$	3.5

Preliminary results from Kaufmann and Gibbs<sup>29</sup> indicate that the largest values of  $|B|/|A|$  at forward angles occur near 50 MeV. Values of this ratio at  $0^\circ$  as a function of beam energy for the DIAS transition in  $(f_{7/2})^n$  configurations are shown in Fig. 18. There is a pronounced peak near 50 MeV. By maximizing the  $|B/A|$  ratio one gains maximum sensitivity to short-range  $N-N$  correlations. This is shown explicitly in Fig. 19, which shows the internucleon range  $r$  involved for both the  $A$  and  $B$  amplitudes. It is seen that  $A$  is relatively flat with  $r$ , whereas  $B$  is sharply peaked at small  $r$ .

From these results, we would conclude that measuring forward-angle DIAS cross sections near 50 MeV is an optimum way to study short-range nucleon correlations.

#### F. New Results on $^{12,14}\text{C}$ and $^{16}\text{O}$

The DCX measurements were extended recently to lower energies for the DIAS transitions of  $^{14}\text{C}$  (Ref. 31) and  $^{16}\text{O}$  (Ref. 32) and the non-analog transition  $^{12}\text{C}(\pi^+, \pi^-)^{16}\text{O}(g.s.)$  (Ref. 33). The angular distributions near 50 MeV for these three  $L = 0$  angular distributions are

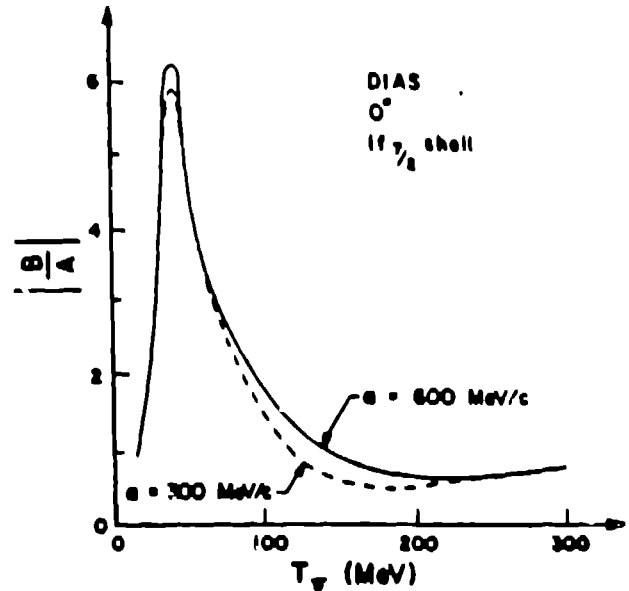


Fig. 18. Theoretical values<sup>29</sup> of the ratios of the two-body transition amplitudes  $|A|$  and  $|B|$  as defined in the text. These were calculated using the theoretical formulation of Ref. 12.

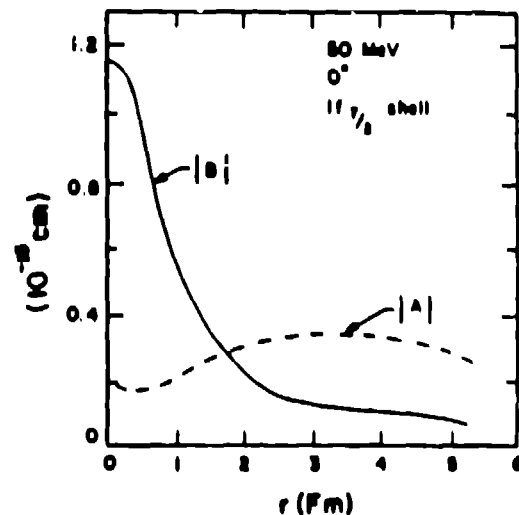


Fig. 19. Theoretical values<sup>29</sup> of  $|A|$  and  $|B|$  (defined in the text) as a function of cutoff radius  $r$ .

shown in Fig. 20. The shapes of the two DIAS angular distributions are seen to be nearly identical. The  $^{12}\text{C}$  angular distribution is forward peaked but the cross sections are smaller by a factor of approximately 5.

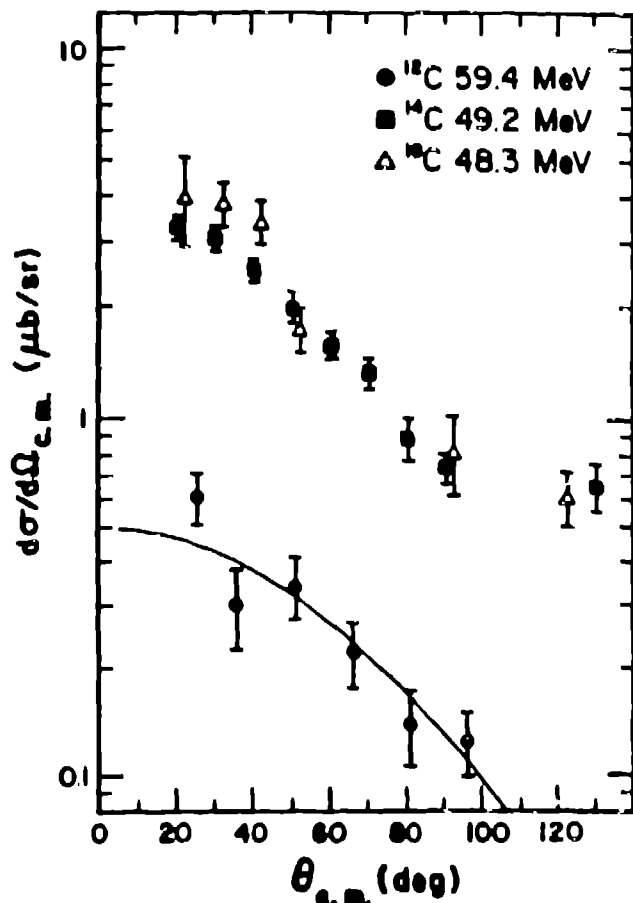


Fig. 20. Measured angular distributions for the  $(\pi^+, \pi^-)$  DIAS transitions in  $^{14}\text{C}$  (Ref. 10) and  $^{16}\text{O}$  (Ref. 32) and for the  $^{12}\text{C}(\pi^+, \pi^-)^{12}\text{O}(\text{g.s.})$  transition (Ref. 33)<sup>†</sup>

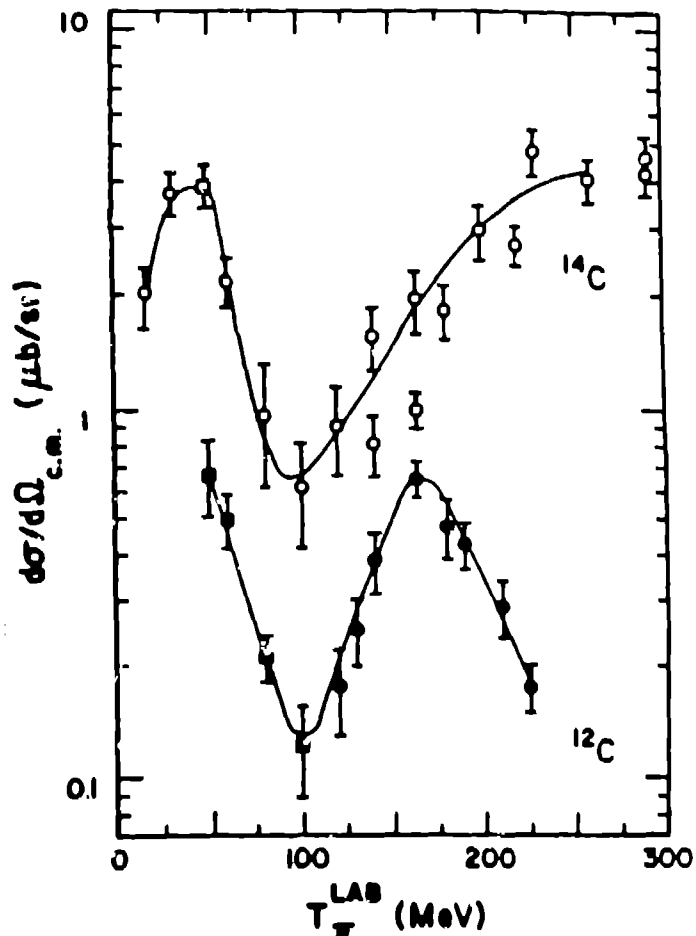


Fig. 21. Forward angle ( $0$  or  $5^\circ$ ) excitation functions for the  $^{14}\text{C}(\pi^+, \pi^-)^{14}\text{O}$  (DIAS) reaction (Ref. 10,31,34,35) and for the  $^{12}\text{C}(\pi^+, \pi^-)^{12}\text{O}(\text{g.s.})$  reaction (Ref. 33).

The forward angle excitation functions for the  $^{12,14}\text{C}(\pi^+, \pi^-)$  transitions are shown in Fig. 21. For  $^{14}\text{C}$ , we recently measured<sup>31</sup> new cross sections at 19.0, 29.1, and 64.4 MeV.

For the latter two energies, angular distributions were measured and extrapolations to  $0^\circ$  could be made. At 19.0 MeV only the cross section at  $40^\circ$  was measured and its value is  $2.0 \pm 0.4$  MeV. The DIAS angular distribution at 19 MeV is expected to be nearly isotropic, so we show the  $40^\circ$  value in Fig. 21. From this datum, we learn that the DIAS excitation function turns over at low energies. The 19 MeV cross section for  $^{14}\text{C}$  is the first measured at this low energy for a DCX reaction, and the  $^{12}\text{C}$  data are the first non-analog cross section measured at  $T_\pi < 80$  MeV.

The new low-energy data are quite interesting. The fact that both the  $^{12}\text{C}$  and  $^{14}\text{C}$  transitions rise with lowering of beam energy forces one to seek an explanation common to both types of transitions. One common factor is the increased pion penetration at low energies, and it most probably is responsible for some of the increase in cross section. A second factor, as given by the theoretical analyses discussed above, is the enhanced scattering amplitude through non-analog intermediate states near 50 MeV (Fig. 18). Since  $^{12}\text{C}$  has no IAS this is the only type of amplitude. Thus it is reassuring to see that the  $^{12}\text{C}$  cross sections are relatively large near 50 MeV. By contrast, at high energies ( $T_\pi \geq 230$ ), the  $^{12}\text{C}$  (and other  $T = 0$  nuclei) have small cross sections. This too supports the theoretical predictions (e.g. Ref. 36) which indicate that the DIAS cross sections at high energies arise predominantly from sequential scattering through the IAS.

If the  $^{12,14}\text{C}$  comparison can be taken as a guide to the role of non-analog intermediate states in DIAS transitions, one would expect a large role for non-analog intermediate states in the  $^{14}\text{C}$  transition at energies near 100 MeV. From Fig. 21 we see that the  $^{12}\text{C}$  transition has a peak at this energy. The origin of this peak is not well-understood at present.

At low pion energies there are Q-value effects that must be taken into account in comparing DIAS and non-DIAS transitions in neighboring  $N = Z$  nuclei. There are large differences, as given below:

Target	Q (MeV) DIAS	Q (MeV) GS
$^{12}\text{C}$		-31.1
$^{14}\text{C}$	-3.97	-3.97
$^{16}\text{O}$		-28.8
$^{18}\text{O}$	-5.08	-5.08

Thus for  $^{12}\text{C}$  a beam energy of 59.4 MeV produces a  $\pi^-$  of energy of 18.3 MeV. For  $^{14}\text{C}$ , a beam energy of 59.4 MeV gives a  $\pi^-$  of energy 55.4 MeV. This difference must be taken into account in detailed comparisons of the two reactions.

#### IV. SUMMARY AND CONCLUSIONS

We have followed in this article the progress in the measurement and analysis of the IAS and DIAS transitions of pion-charge exchange reactions at low energies. I believe we have the following results.

- (1) IAS transitions: Recent measurements now determine quite well the patterns of the forward-angle cross sections in the energy range 20 to 500 MeV for nuclei from  $^1\text{H}$  to  $^{208}\text{Pb}$ . These data serve to characterize the isovector part of the pion-nucleus interaction. At low pion energies the forward-angle IAS cross sections exhibit a deep minimum near 50 MeV, a feature originating in the free  $\pi^-p \rightarrow \pi^0n$  cross sections. Its persistence in  $\pi$ -A scattering places strong constraints on dispersive-medium effects.
- (2) DIAS transitions: There now exists an extensive body of data at energies 20 to 300 MeV that establishes the systematics of forward-angle cross sections. Interest in these data continues to center on the unambiguous identification of the role of short-range N-N correlations. At low pion energies, the observed forward-peaked angular distributions seem to be signatures of short-range effects. The anomalous cross section ratios for  $^{42,44,48}\text{Ca}$  can be understood as being a consequence of the short-range nature of the DCX process, and indeed give strong support to such a conclusion. Although quark degrees of freedom have been employed to describe short-range features of DCX reactions, to date there is no unique signature to the role of quarks. One can hope that as more conventional analyses provide an unambiguous identification of the short-range components in DCX reactions, the role of quark degrees of freedom may be seen.

## REFERENCES

1. Calculated using the  $\pi - N$  phase shift code SAID, R. Arndt, Virginia Polytechnic Institute and State University.
2. D. H. Fitzgerald, H. W. Baer, J. D. Bowman, M. D. Cooper, F. Irom, N. S. P. King, M. J. Leitch, E. Piasetzky, W. J. Briscoe, M. E. Sadler, K. J. Smith, and J. N. Knudson, *Phys. Rev. C* **34**, 619 (1986).
3. D. F. Measday, in these Proceedings.
4. H. W. Baer, R. D. Bolton, J. D. Bowman, M. D. Cooper, F. H. Cverna, R. H. Heffner, C. M. Hoffman, N. S. P. King, J. Piffaretti, J. Alster, A. Doron, S. Gilad, M. A. Moinester, P. R. Bevington, and E. Winkelmann, *Nuclear Instruments and Methods* **180**, 445 (1981).
5. J. L. Ullmann, P. W. F. Alons, J. J. Kraushaar, J. H. Mitchell, R. J. Peterson, R. A. Ristinen, J. N. Knudson, J. R. Comfort, H. W. Baer, J. D. Bowman, M. D. Bowman, M. D. Cooper, D. H. Fitzgerald, F. Irom, M. J. Leitch, and E. Piasetzky, *Physical Review C* **33**, 2092 (1986).
6. F. Irom, M. J. Leitch, H. W. Baer, J. D. Bowman, M. D. Cooper, B. J. Dropesky, E. Piasetzky, and J. N. Knudson, *Physical Review Letters* **55**, 1862 (1985).
7. M. J. Leitch, H. W. Baer, J. D. Bowman, M. D. Cooper, E. Piasetzky, U. Sennhauser, H. J. Ziock, F. Irom, P. B. Siegel, and M. A. Moinester, *Phys. Rev. C* **33**, 278 (1986).
8. F. Irom, H. W. Baer, A. G. Bergmann, J. D. Bowman, P. Heusi, D. H. Fitzgerald, C. J. Sefor, M. E. Sadler, J. N. Knudson, W. J. Briscoe, P. W. F. Alons, E. Piasetzky, and S. H. Rokni, *Physical Review C* (in press).
9. G. A. Miller, *Physical Review Letters* **53**, 2008 (1984).
10. M. J. Leitch, E. Piasetzky, H. W. Baer, J. D. Bowman, R. L. Burman, B. J. Dropesky, P. A. M. Gram, F. Irom, D. Roberts, G. A. Rebka, Jr, J. N. Knudson, J. R. Comfort, V. A. Plinnick, D. H. Wright, and S. A. Woods, *Physical Review Letters* **54**, 1482 (1985).
11. G. A. Miller, in *Proceedings of the LAMPF Workshop on Pion Double Charge Exchange, January 1985*, Los Alamos National Laboratory report LA-10550-C (H. W. Baer and M. J. Leitch, Eds.), p. 193.
12. W. R. Gibbs, W. B. Kaufmann, and P. B. Siegel, *Workshop*, loc. cit., p. 90.
13. E. R. Siciliano, *Workshop*, loc. cit., p. 180.
14. E. R. Siciliano, M. D. Cooper, M. B. Johnson, and M. J. Leitch, *Physical Review C* **34**, 267 (1986).

15. L. C. Liu, Workshop, loc. cit., p. 109.
16. T. Karapiperis and M. Kobayashi, *Physical Review Letters* **54**, 1230 (1985); SIN preprint PR-85-04 (1985); and Abstract, Book I, Sixth International Conference on Particles and Nuclei, Kyoto, Japan, April 1987 (PANIC'87), p. 368.
17. M. B. Johnson and E. R. Siciliano, *Physical Review* **C27**, 730 (1983), and *Physical Review* **C27**, 1647 (1983).
18. G. A. Miller and J. E. Spencer, *Annals of Physics* **100**, 562 (1976).
19. E. Oset and D. Strottman, *Nuclear Physics* **A355**, 437 (1981).
20. T. Karapiperis, M. Kobayashi, and M. Hirata, *Physics Letters* **144B**, 23 (1984).
21. E. Oset, D. Strottman, M. J. Vicente-Vacas, Ma Wei-Hsing, *Nuclear Physics* **A408**, 461 (1983).
22. M. B. Johnson and L. S. Kisslinger, *Physics Letters* **168B**, 26 (1986).
23. M. Bleszynski and R. Glauber, *Phys. Rev.* **C36**, 681 (1987).
24. S. Cohen and D. Kurath, *Nuclear Physics* **73**, 1 (1965).
25. H. W. Baer, M. J. Leitch, R. L. Burman, M. D. Cooper, A. Z. Cui, B. J. Dropesky, G. C. Giesler, F. Irom, C. L. Morris, J. N. Knudson, J. R. Comfort, D. H. Wright, and R. Gilman, *Physical Review* **C35**, 1425 (1987).
26. Z. Weinfeld, E. Piassetzky, H. W. Baer, R. L. Burman, M. J. Leitch, C. L. Morris, D. H. Wright, S. H. Rokni, and J. R. Comfort, Los Alamos preprint LA-UR-87-1073 (1987); also PANIC'87 loc. cit., p. 364.
27. D. S. Koltun and A. Reitan, *Physical Review* **139**, B1372 (1965).
28. E. Bleszynski, M. Bleszynski, and R. Glauber, PANIC'87, loc. cit., p. 358.
29. W. B. Kaufmann and W. R. Gibbs, private communication, 1987; calculations are based on the theory of Ref. 44.
30. N. Auerbach, W. R. Gibbs, and E. Piassetzky, Los Alamos preprint LA-UR-86-4283 (1986); also PANIC'87, *ibid.*, p. 366.
31. M. J. Leitch, H.-W. Baer, R. L. Burman, M. D. Cooper, B. J. Dropesky, F. Irom, C. L. Morris, J. N. Knudson, J. R. Comfort, D. H. Wright, R. Gilman, E. Piassetzky, and Z. Weinfeld (to be published).
32. A. Altman, R. R. Johnson, U. Wienands, N. Hessey, B. M. Barnett, B. M. Forster, N. Grion, D. Mills, F. M. Rozon, G. R. Smith, R. P. Trelle, D. R. Gill, G. Sheffer, and T. Anderl, *Physical Review Letters* **55**, 1273 (1985).

33. J. A. Faucett, M. W. Rawool, K. S. Dhuga, J. D. Zumbro, R. Gilman, H. T. Fortune, C. L. Morris, and M. A. Plum, *Phys. Rev. C***35**, 1570 (1987).
34. P. A. Seidl, M. D. Brown, R. R. Kiziah, C. F. Moore, H. W. Baer, C. L. Morris, G. R. Burleson, W. B. Cottingham, S. J. Greene, L. C. Bland, R. Gilman, and H. T. Fortune, *Physical Review C***30**, 973 (1984).
35. DCX data compilation by R. Gilman, Ph.D. dissertation, University of Pennsylvania, 1985 (Los Alamos report LA-10524-T).
36. G. A. Miller, *Phys. Rev. C***24**, 221 (1981).

## FIGURE CAPTIONS

- Fig. 1. Angular distributions for the  $\pi^-p \rightarrow \pi^0n$  reactions at three energies, as given by a current phase shift analysis (Ref. 1).
- Fig. 2. Angular distributions for the  $\pi^-p \rightarrow \pi^0n$  reactions at three low energies (Ref. 1).
- Fig. 3. The  $0^\circ$  cross sections as a function of incident energy for the  $\pi^-p \rightarrow \pi^0n$  reaction (Ref. 1).
- Fig. 4. Spectra for the  $^{14}\text{C}(\pi^+, \pi^0)$  reaction measured<sup>6</sup> at forward angles (0 to  $10^\circ$ ) at different energies. The IAS is seen to disappear at 50 MeV.
- Fig. 5. The energy dependence of  $0^\circ$  IAS cross sections on  $^{14}\text{C}$  (Ref. 5). The solid line represents two times the free  $\pi^-p \rightarrow \pi^0n$  cross section. The dashed line represents the multiple scattering theory calculations of Kaufmann *et al.* as discussed in Ref. 5.
- Fig. 6. The measured  $0^\circ$  excitation functions for the IAS transition at low pion energies.<sup>6</sup> The solid lines represent polynomial fits to the data used to determine the energy of the minima in the cross sections.
- Fig. 7. Angular distributions for the IAS transition on  $^{15}\text{N}$  at three low energies.<sup>6,7</sup> The curves represent the polynomial function fits to the data used to determine  $0^\circ$  cross sections.
- Fig. 8. Angular distributions at 20 MeV for the IAS transitions on  $^7\text{Li}$  and  $^{14}\text{C}$  (Ref. 8). The solid curves are DWIA calculations including the Coulomb force on the incident pion. The dotted curve is for the same calculations with the Coulomb force turned off.
- Fig. 9-19. Figure caption 9-19 are given in the text.
- Fig. 20. Measured angular distributions for the  $(\pi^+, \pi^-)$  DIAS transitions in  $^{14}\text{C}$  (Ref. 10) and  $^{16}\text{O}$  (Ref. 32) and for the  $^{12}\text{C}(\pi^+, \pi^-)^{12}\text{O}(\text{g.s.})$  transition (Ref. 33).
- Fig. 21. Forward angle (0 or  $5^\circ$ ) excitation functions for the  $^{14}\text{C}(\pi^+, \pi^-)^{14}\text{O}(\text{DIAS})$  reaction (Ref. 10, 31, 34, 35) and for the  $^{12}\text{C}(\pi^+, \pi^-)^{12}\text{O}(\text{g.s.})$  reaction (Ref. 33).